J Biomol NMR (2011) 51:477–485
DOI 10.1007/s10858-011-9578-1

ARTICLE

Three-dimensional deuterium-carbon correlation experiments for high-resolution solid-state MAS NMR spectroscopy of large proteins

Daniela Lalli · Paul Schanda · Anup Chowdhury · Joren Retel · Matthias Hiller · Victoria A. Higman · Lieselotte Handel · Vipin Agarwal · Bernd Reif · Barth van Rossum · Ümit Akbey · Hartmut Oschkinat

Received: 3 August 2011 / Accepted: 23 September 2011 / Published online: 25 October 2011

Abstract Well-resolved ^{2}H–^{13}C correlation spectra, reminiscent of ^{1}H–^{13}C correlations, are obtained for perdeuterated ubiquitin and for perdeuterated outer-membrane protein G (OmpG) from *E. coli* by exploiting the favorable lifetime of ^{2}H double-quantum (DQ) states. Sufficient signal-to-noise was achieved due to the short deuterium T_1, allowing for high repetition rates and enabling 3D experiments with a ^{2}H–^{13}C transfer step in a reasonable time. Well-resolved 3D $^{2}H_{DQ}$–^{13}C–^{13}C correlations of ubiquitin and OmpG were recorded within 3.5 days each. An essentially complete assignment of $^{2}H_{DQ\alpha}$ shifts and of a substantial fraction of $^{2}H_{DQ\beta}$ shifts were obtained for ubiquitin. In the case of OmpG, $^{2}H_{DQ\alpha}$ and $^{2}H_{DQ\beta}$ chemical shifts of a considerable number of threonine, serine and leucine residues were assigned. This approach provides the basis for a general heteronuclear 3D MAS NMR assignment concept utilizing pulse sequences with $^{2}H_{DQ}$–^{13}C transfer steps and evolution of deuterium double-quantum chemical shifts.

Keywords Solid-state NMR · Micro-crystalline · Membrane proteins · Ubiquitin · OmpG · Deuterium-carbon correlations

Introduction

A MAS NMR structure determination concept applicable to large, solid-like biological systems (membrane proteins and their complexes in native lipid bilayers, cytoskeleton-

Electronic supplementary material The online version of this article (doi:10.1007/s10858-011-9578-1) contains supplementary material, which is available to authorized users.

D. Lalli · A. Chowdhury · J. Retel · M. Hiller · V. A. Higman · L. Handel · V. Agarwal · B. Reif · B. van Rossum · Ü. Akbey · H. Oschkinat (✉)
Leibniz-Institut für Molekulare Pharmakologie (FMP), Robert-Rössle-Strasse 10, 13125 Berlin, Germany
e-mail: oschkinat@fmp-berlin.de

D. Lalli
Magnetic Resonance Center and Department of Chemistry, University of Florence, Via Luigi Sacconi 6, 50019 Sesto Fiorentino, Italy

P. Schanda
Physical Chemistry, ETH Zürich, Wolfgang-Pauli-Strasse 10, 8093 Zurich, Switzerland

P. Schanda (✉)
Institut de Biologie Structurale, Jean-Pierre Ebel C.N.R.S.-C.E.A.-UJF, 41, rue Jules Horowitz, 38027 Grenoble Cedex 1, France
e-mail: paul.schanda@ibs.fr

V. A. Higman
Department of Biochemistry, University of Oxford, South Park Road, Oxford OX1 3QU, UK

V. Agarwal
Department of Chemistry, Radboud University, Toernooiveld 1, 6525 ED Nijmegen, The Netherlands

B. Reif
Fachbereich Chemie, Technische Universität München, Lichtenbergstr. 4, 85747 Garching, Germany

attached proteins, fibrilar and polydisperse oligomers) (Castellani et al. 2002; Jehle et al. 2010; Lange et al. 2006; Rienstra et al. 2002; Wasmer et al. 2008) requires multi-dimensional NMR experiments using chemical shifts of several different nuclei to resolve complex NMR-spectra. In solution NMR, this is achieved by exploiting ^{1}H, ^{13}C and ^{15}N chemical shifts in three- (3D) and higher dimensional experiments (Sattler et al. 1999). The chemical shifts of the C_α and C_β signals are specific for certain amino acid types and the chemical shift dispersion is often large compared to the line width. Thus, correlating C_β chemical shifts with those of backbone proton, carbon and nitrogen nuclei provides the basis for the sequential assignment. Side-chain assignments are obtained from 3D HCCH–COSY or HCCH–TOCSY-type spectra where considerable resolution is provided by a proton frequency axis (Bax et al. 1990a, b; Fesik et al. 1990; Ikura et al. 1991; Kay et al. 1990). Investigations of large proteins are facilitated by deuteration of non-exchangeable sites. Furthermore, in the applied pulse sequences the magnetization of all side chain carbons are relayed to the backbone –NH protons which are then usually detected (Bax and Grzesiek 1993; Grzesiek and Bax 1992).

In MAS NMR experiments of solid-like biological samples, however, the proton signals are notoriously broad due to the strong dipolar couplings in extended networks of proton spins, even when applying high magic-angle spinning frequencies (Schnell and Spiess 2001). To be able to use amide proton chemical shifts in solid-state assignment strategies, Reif and co-workers (Chevelkov et al. 2006) have recently proposed recording solution-like backbone correlation experiments, enabling magnetization transfers via scalar couplings and/or cross polarization (Linser et al. 2008). For this purpose, perdeuterated protein samples were prepared in which 10% of the amide protons are back-exchanged using 10/90% H_2O/D_2O as solvent. As a result, line widths of $\sim$19 and $\sim$11 Hz for amide proton and nitrogen signals, respectively, were observed, enabling magnetization transfers via scalar couplings (Linser et al. 2008). Using higher proton content (up to 100% back-exchanged) and moderate spinning frequency (24 kHz), CP-based transfers enable the use of amide proton chemical shifts at still moderate proton line width. However, in contrast to solution NMR, where the *J*-based magnetization transfers are very efficient in so-called 'out-and-back' experiments in conjunction with protein deuteration (Archer and Bax 1991), the application of an equal number of cross-polarization steps in solid-state MAS NMR pulse sequences is undesired since costly with regards to signal-to-noise. It would be of tremendous advantage to excite side-chain carbon resonances via deuterium in a more direct manner to achieve, for example, the transfer $D \rightarrow C_\beta \rightarrow C_\alpha \rightarrow NH$, applying proton detection. In principle, a particular advantage of solid-state NMR could be exploited for this purpose by directly starting from the sidechains without a lengthy out-and-back approach and by making use of deuterium double-quantum frequencies (Agarwal et al. 2009).

Here, we present 2D $^{2}H_{DQ}$–^{13}C and 3D $^{2}H_{DQ}$–^{13}C–^{13}C correlations for the identification of amino-acid side-chain spin systems using perdeuterated samples of microcrystalline ubiquitin and OmpG in native lipid bilayers. Deuterium double-quantum evolution is employed prior to heteronuclear cross polarization to achieve sufficient resolution (Agarwal et al. 2009; Chandrakumar et al. 1994; Kristensen et al. 1999). The $^{2}H_{DQ}$–^{13}C–^{13}C spectrum is valuable for resolving the carbon signal pattern in cases of strong overlap of ^{13}C–^{13}C correlation signals, taking advantage of the chemical shift dispersion in the additional dimension. Its usefulness is demonstrated with the resolution of threonine, serine and leucine side chain signals of OmpG.

Experimental

Protein samples

Uniformly $^{2}H/^{13}C/^{15}N$ labeled human ubiquitin was expressed and purified using standard protocols. Protein microcrystals were grown at 4°C with the sitting drop method and a crystallization buffer containing 20% of H_2O and 80% D_2O, following the procedure described by Igumenova et al. (2004). About 15 mg of protein were transferred into a 2.5 mm rotor using an ultracentrifuge device (Bockmann et al. 2009).

Uniformly $^{2}H/^{13}C/^{15}N$ labeled OmpG was prepared as described by Hiller et al. (2005). In order to obtain a deuterated sample, the protein was expressed as inclusion bodies using fully deuterated M9 minimal medium containing u-[^{2}H,^{13}C]-glucose and ^{15}N–NH_4Cl as sole carbon and nitrogen sources, respectively. After purification under denaturing conditions (8 M urea), the proton content of the backbone amide was set to 30%. Native OmpG was obtained by refolding the protein in a detergent-containing buffer. For this purpose, a 1 mM solution from lyophilized dodecyl-β-D-maltoside was prepared using the refolding buffer (30% H_2O and 70% D_2O). Similarly, the buffer for the subsequent reconstitution and 2D crystallization also contained 30% H_2O and 70% D_2O.

NMR spectroscopy

NMR experiments on ubiquitin were performed on a Bruker Avance 600 wide-bore spectrometer operating at 14.09 T equipped with a 2.5 mm triple-resonance Chemagnetics HXY probe. The MAS frequency was set to

25 kHz and stabilized to within 10 Hz. The cooling air was cooled at −15°C, and the effective sample temperature was estimated to be about 10−15°C. NMR experiments on OmpG were recorded on a Bruker Avance 600 wide-bore spectrometer with a triple resonance Bruker 3.2 mm HXY probe. The spectra were recorded at 20 kHz MAS and with a flow gas temperature of 0°C.

For the 2D $^{2}H_{DQ}$–^{13}C correlation experiments the rf field amplitude for hard pulses was adjusted to 100 kHz for ^{13}C and 104 kHz (the maximum achievable with the hardware) for ^{2}H, setting the rf carrier to 100 and 1.2 ppm, respectively. For ^{2}H–^{13}C CP the contact time was set to 1.4 ms. The ^{2}H field during CP was ramped from 95 to 105 kHz and the ^{13}C field was matched to the (−1) Hartmann-Hahn condition (approximately 75 kHz). The DQ generation/reconversion delay τ was set to 1 μs to yield efficient DQ excitation for $^{2}H_{DQ\alpha}$. The z-filter delay Δ was set to 2 μs. The spectral width was 50 and 3.125 kHz for the direct and indirect dimension, thus ensuring that the ^{2}H dwell time is an integer multiple of the rotor period. 4,096 and 160 points corresponding to acquisition times of 41.0 ms (^{13}C) and 25.6 ms (^{2}H) were acquired in t_1 and t_2, respectively. 1,024 transients were acquired per t_1 increment. The recycle delay was set to 150 ms leading to an acquisition time of about 9 h. WALTZ-16 decoupling on the ^{2}H channel was applied using rf field strength of 3 kHz (Shaka et al. 1983).

The 3D $^{2}H_{DQ}$–^{13}C–^{13}C correlation experiments were recorded with the pulse sequence shown in Fig. 1. In this pulse sequence, the first two 90° hard pulses, with a duration of 2.4 μs and separated by a delay ($\tau = 1$ μs) generate the DQ coherence that evolves in the t_1 dimension. A time reversal approach is adopted to convert the DQ coherence back to SQ transverse magnetization. The fourth 90° pulse flips the deuterium magnetization along the z-axis followed by a 2 μs z-filter delay. The fifth ^{2}H 90° brings the magnetization back to the xy-plane. For the following ^{2}H–^{13}C CP, a contact time of 1.5 ms was used. The ^{2}H rf field during CP was ramped from 91 to 101 kHz and the ^{13}C field was matched to the (−1) Hartmann-Hahn condition (approximately 71 kHz). The WALTZ-16 decoupling on the ^{1}H and ^{2}H channels during the ^{13}C evolution (t_2) and the detection (t_3) period was set to a field strength of 3 kHz. The rf amplitude during the 5 ms DREAM recoupling period was tangentially swept setting the mean rf field amplitude according to half the spinning frequency and using a Δ_{rf} and d_{est} values of 5.6 and 2 kHz, respectively (Verel et al. 2001). The mean rf value was optimized within a small range in order to have maximal transfer. The spectral width was 50, 18 and 3.125 kHz for t_3 (^{13}C), t_2 (^{13}C) and t_1 (^{2}H) dimensions, respectively. 2,048, 250 and 32 points corresponding to acquisition times of 20.5, 6.9 and 5.1 ms were acquired in t_3, t_2 and t_1 respectively. 160 transients were acquired per t_1 increment. The recycle delay was set to 150 ms leading to an acquisition time of about 3 days. Spectra were processed with the program TopSpin 2.0 (Bruker). The 2D and 3D maps were analyzed with the CARA 1.8.4.2 program (Keller and Wuthrich 2002).

Assignment of human ubiquitin

Deuterium resonance assignments of ubiquitin was carried out starting from the reported assignment on BMRB entry 7111 (Schubert et al. 2006).

Results

Figure 2 shows a $^{2}H_{DQ}$–^{13}C correlation spectrum obtained for deuterated ubiquitin (∼15 mg), measured at a 25 kHz MAS frequency using a previously proposed pulse

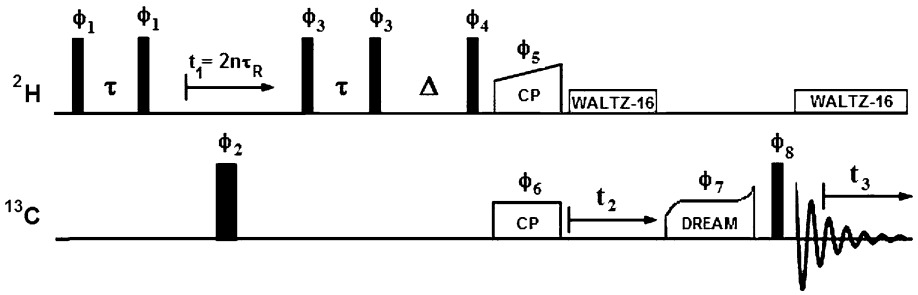

Fig. 1 Schematic representation of the pulse scheme employed in this study for recording the three-dimensional $^{2}H_{DQ}$–^{13}C–^{13}C correlation experiment. *Narrow rectangles* represent 90° pulses, while the *wide rectangle* represents a 180° pulse. The double-quantum excitation-evolution-reconversion period for the first t_1-increment is equal to one rotor period: $\tau_R = 3*\tau_{90°} + 2*\tau + t_1(0)$, where $\tau_{90°} = {}^{2}H$ 90° pulses, $\tau_{180°} = {}^{13}C$ 180° pulse, τ = free evolution period and $t_1(0)$ = deuterium evolution period for the first increment. All increments in the indirect dimension were adjusted as multiple of the rotor period: $t_1 = 2n*\tau_R$ with n as integer number. Phase cycling: $\phi_1 = (x, y, -x, -y)$; $\phi_2 = (-y)$; $\phi_3 = (x)$; $\phi_4 = (4(x), 4(-x))$; $\phi_5 = (y)$; $\phi_6 = (8(x), 8(-x))$; $\phi_7 = (16(x), 16(-x))$; $\phi_8 = (2(x), 4(-x), 2(x))$; $\phi_{REC} = (2(x, -x), 4(-x, x), 2(x, -x))$. Phase sensitive detection in t_1 and t_2 is achieved using TPPI on phase ϕ_1 and ϕ_6, respectively

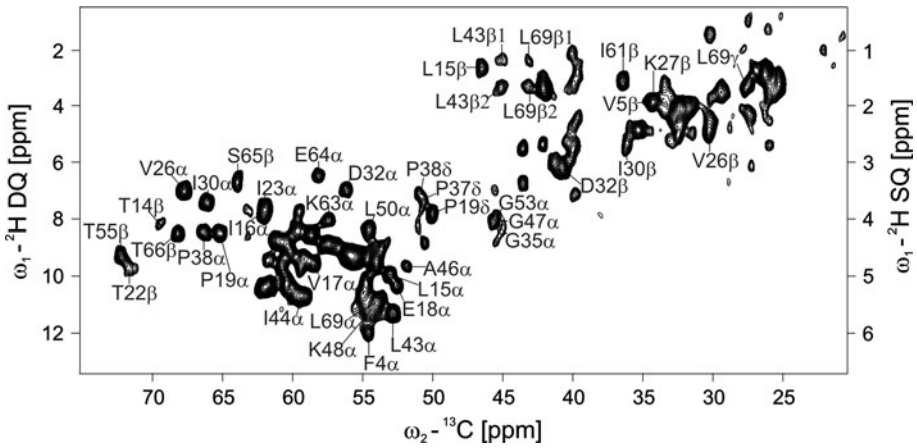

Fig. 2 $^{2}H_{DQ}$–^{13}C correlation spectrum of uniformly $^{2}H/^{13}C/^{15}N$ labeled ubiquitin, back-exchanged to ^{1}H at 20% of the exchangeable sites. The $^{2}H_{DQ}$ chemical shift as well as the calculated $^{2}H_{SQ}$ chemical shift are reported. The spectrum was processed with a squared sine function with a phase shift of $\pi/5$ in the indirect dimension while a Gauss-Lorentz function in the direct dimension was applied using exponential line broadening of −40 Hz and a Gaussian maximum of 0.1

Table 1 List of ^{2}H linewidths and signal-to-noise ratios for different ^{2}H–^{13}C moieties observed in the $^{2}H_{DQ}$–^{13}C correlation spectrum of ubiquitin

Amino acid	^{2}H DQ linewidth (Hz)	S/N
F4α	47.5	7.6
L15β	48.3	7.1
P19α	38.7	13.2
V26α	42.0	12.9
I30α	40.9	13.5
D32α	47.0	8.7
P38α	38.6	10.2
A46α	36.5	8.2
I61β	47.3	8.1
K63α	39.9	10.0
E64α	40.3	6.4
S65β	51.3	9.3
T66β	34.8	15.0

sequence (Agarwal et al. 2009). Well-resolved correlation peaks of the types $^{2}H_{DQ\alpha}$–$^{13}C_{\alpha}$ and $^{2}H_{DQ\beta}$–$^{13}C_{\beta}$ are obtained. The typical deuterium line width associated with the $^{2}H_{DQ\alpha}$–$^{13}C_{\alpha}$ peaks is about 36–50 Hz (~0.4–0.5 ppm) (Table 1), with the narrowest ^{2}H DQ linewidth (36.5 Hz) observed for the $^{2}H_{\alpha}$ of A46. As an interesting feature, the chemical shifts of the geminal deuterons at C_{β} of leucines 43 and 69 can be identified easily (see Fig. 2). The spectrum shows ample signal-to-noise (S/N, $\cong$ 10.1 ± 0.6, average) and all expected $^{2}H_{DQ\alpha}$–$^{13}C_{\alpha}$ signals are present. The spectrum was recorded with a maximum ^{2}H evolution time of 25.6 ms, aiming thereby at maximum resolution (9 h experimental time). Processing of a reduced number of t_1-experiments showed that spectra with sufficient resolution and S/N can in fact be obtained after 1–2 h (see supplementary information, SI1). The time of $^{2}H_{DQ}$ generation has been set to an optimum length for signals of nuclei with relatively large quadrupolar couplings, in particular $^{2}H_{DQ\alpha}$ and $^{2}H_{DQ\beta}$. The optimal time for $^{2}H_{DQ}$ excitation is inversely proportional to the size of the quadrupolar coupling constant. Due to the methyl group rotation, the quadrupolar coupling constant of the methyl deuterons ($e^2qQ/\hbar = 55$ kHz) is relatively small compared to that of $^{2}H_{DQ\alpha}$ ($e^2qQ/\hbar = 165$ kHz). Therefore the methyl deuteron signals are less well excited.

For the generation/reconversion of $^{2}H_{\alpha}$ DQ coherences in ubiquitin we found a mid-pulse to mid-pulse period of 3.4 μs appropriate, using pulses of 2.4 μs in length and a 1 μs delay. The excitation of double-quantum coherences involving methyl deuterons required a delay of 9 μs, using the same pulse length (Agarwal et al. 2009).

The optimized settings for C_{α} excitation were used in a 3D $^{2}H_{DQ}$–^{13}C–^{13}C correlation experiment together with the DREAM recoupling scheme to establish ^{13}C–^{13}C connectivities (Verel et al. 2001). In contrast to techniques relying on the presence of proton spins, such as PAR (De et al. 2008), DARR (Takegoshi et al. 2003), or MIRROR (Scholz et al. 2008), the DREAM scheme performs a first-order recoupling of the homonuclear ^{13}C–^{13}C dipolar coupling leading to good results with perdeuterated samples, however, for a limited bandwidth. While other mixing sequences such as RFDR (Bennett et al. 1992), C7 (Lee et al. 1995), or DONER (Akbey et al. 2009; Leskes et al. 2011) could be used for deuterated samples as well, we have chosen the DREAM recoupling sequence (Huang et al. 2011). This leads to strong cross-peaks which are, however, asymmetric on both sides of the diagonal. To achieve a more symmetric cross-peak pattern, RFDR- or DONER-type sequences maybe used, and maybe also the DQ excitation-reconversion time can be optimized for observation of different carbon sites. Furthermore, fast spinning would make the DREAM transfer more broadband, and our experiment would thus provide more symmetric spectra (Ernst et al. 2003). At fast MAS, INEPT-type transfer between carbons will also be a viable option, as transverse dephasing times of carbons are expected to become long. Figure 1 shows the pulse sequence used for

the 3D $^{2}H_{DQ}$–^{13}C–^{13}C experiment. After initial generation of deuterium DQ coherences, chemical shift evolution and reconversion, the deuterium single-quantum magnetization is transferred to the directly bonded carbon. After ^{13}C chemical shift evolution, the carbon–carbon mixing element then establishes strong one-bond and, to a lesser extent, long-range transfers. The two most valuable spin patterns for the assignment procedure consist of cross peaks with the frequencies of $^{2}H_{DQ\alpha i}$–$^{13}C_{\alpha i}$–$^{13}C_{Xi}$ or $^{2}H_{DQ\beta i}$–$^{13}C_{\beta i}$–$^{13}C_{Xi}$ where $^{13}C_{Xi}$ can be one of the carbon spins of residue i (CO, $C_{\alpha i}$, $C_{\beta i}$ etc.).

A cube representation of the 3D $^{2}H_{DQ}$–^{13}C–^{13}C correlation spectrum obtained on ubiquitin is shown in Fig. 3a. The asymmetry of the spectrum is a result of (i) the lower efficiency of exciting DQ coherences of $^{2}H_{\beta/\delta}$ (smaller quadrupolar coupling than for $^{2}H_{\alpha}$) and (ii) an offset dependency of the DREAM mixing; the rf carrier during the DREAM sweep was centered close to the C_{α} frequency (50 ppm). In Fig. 3b, vertical strips (portions of a ^{13}C–^{13}C plane taken at appropriate $^{2}H_{DQ}$ and ^{13}C-frequencies in F_1 and F_2, respectively) are visualized next to one another to identify desired correlations. The opposite sign of cross and diagonal peak intensities is a result of the double-quantum transfer during DREAM. An evaluation of the information content of the spectrum using existing carbon assignments (BMRB deposition number 7111) was easily possible. By linking the respective cross peaks in the $^{2}H_{DQ}$–^{13}C–^{13}C spectrum, all $^{2}H_{DQ\alpha}$ signals corresponding to the residues 2–70 (Met1 and residues corresponding to 71–76 were not observed), 67% of the $^{2}H_{DQ\beta}$ signals and a few $^{2}H_{DQ\gamma}$ signals were assigned. Examples are shown in Fig. 4, including residues with two deuterons at the β-position. In general, transfers of the type $^{2}H_{DQ\alpha}$–$^{13}C_{\alpha}$–$^{13}C_{\beta/\gamma}$ appeared to be strong, whereas correlations of the type $^{2}H_{DQ\beta}$–$^{13}C_{\beta}$–$^{13}C_{\alpha/\gamma}$ lead to weak cross peaks which were observable in many cases but not all. For leucines, correlations involving methyl group carbon signals were obtained.

In most strips taken at the frequencies of the $^{2}H_{DQ\alpha}$ and $^{13}C_{\alpha}$, cross peaks indicating C_{β} chemical shifts were present. The reverse, the identification of cross peaks originating from $^{2}H_{DQ\beta}$–$^{13}C_{\beta}$–$^{13}C_{\alpha/\gamma}$ transfers was not successful in all cases. On the other hand, C_{β} and C_{γ} could be identified in the $^{2}H_{DQ\alpha}$–$^{13}C_{\alpha}$ and $^{2}H_{DQ\delta}$–$^{13}C_{\delta}$ strips. For all of the prolines, it was also possible to recognize the $^{2}H_{DQ\delta}$–$^{13}C_{\delta}$ signals which are important for sequential assignment procedures. For none of the Gln and Glu spin systems, cross peaks due to a $^{2}H_{DQ\beta}$–$^{13}C_{\beta}$–$^{13}C_{\alpha/\gamma}$ transfer were identified. However, in each case, the frequency of the C_{β} was usually found in the $^{2}H_{DQ\alpha}$–$^{13}C_{\alpha}$ strip. Besides these, the $^{2}H_{DQ\beta}$ of Ile3, Lys48, Ser57, Tyr59 were not identified, most likely due to low S/N.

To test the utility of this approach in structure determination projects of large biological systems, the respective 2D and 3D correlations were recorded on a perdeuterated sample of the 281-residue membrane protein OmpG. As expected, the 2D spectrum (Fig. 5a) is considerably more crowded compared to the spectrum of the 76-residue ubiquitin, but the $^{2}H_{DQ}$ line width is still small compared to the chemical shift dispersion. Resolution-optimized processing of the spectrum results in a relatively well-resolved $^{2}H_{DQ\alpha}$–$^{13}C_{\alpha}$ region (Fig. 5b). Inspection of isolated 2D cross peaks in a spectrum processed without resolution enhancement in t_1 revealed $^{2}H_{DQ}$ line widths in the range of 70–100 Hz ($\sim$0.8–1.1 ppm).

A $^{2}H_{DQ\alpha}$–$^{13}C_{\alpha}$ plane taken from the 3D $^{2}H_{DQ}$–^{13}C–^{13}C spectrum (Fig. 6) at 58.2 ppm demonstrates that the resolving power of the deuterium DQ dimension may be

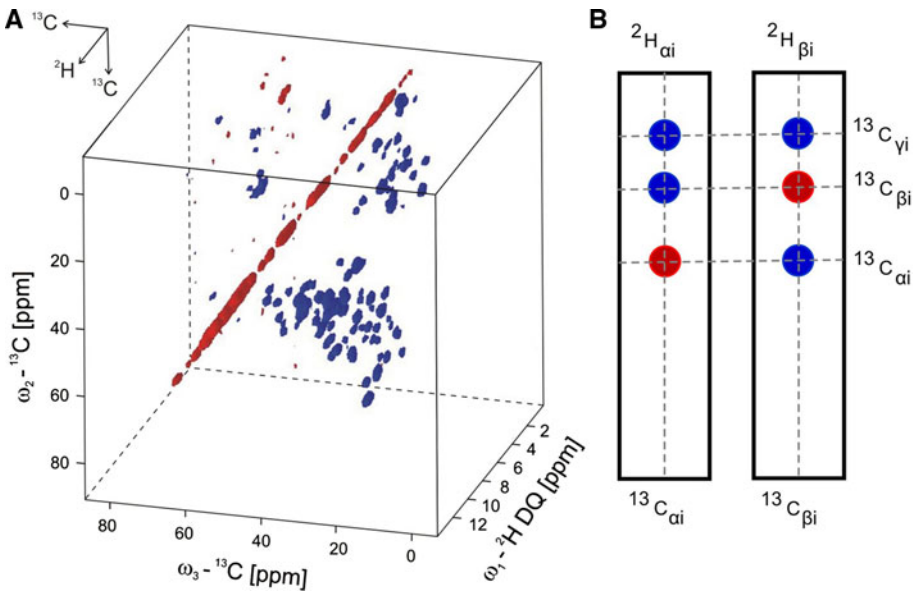

Fig. 3 **a** Cube representation of the three-dimensional $^{2}H_{DQ}$–^{13}C–^{13}C correlation spectrum of the uniformly $^{2}H/^{13}C/^{15}N$ labeled ubiquitin which was back exchanged in a 20/80% H_2O/D_2O solution. **b** Schematic representation of the possible connectivities detected in the 3D $^{2}H_{DQ}$–^{13}C–^{13}C experiments

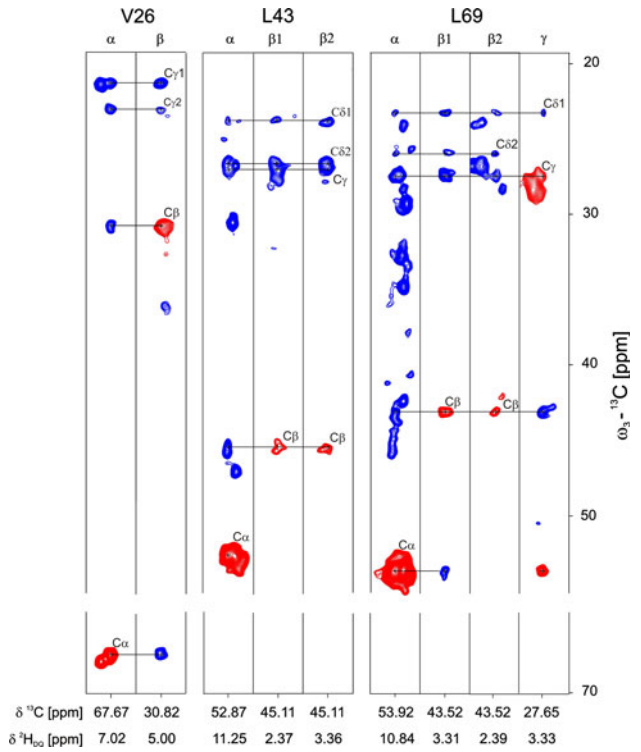

Fig. 4 Representative strip plots of the $^{2}H_{DQ}$–^{13}C–^{13}C spectrum of ubiquitin, showing intra-residue connectivities for residues V26, L43 and L69. *Blue* and *red* peaks are negative cross peaks and positive diagonal peaks respectively. Each strip is extracted at the ^{13}C frequency reported at the *bottom*. The $^{2}H_{DQ}$ frequency of the plane from which strips are extracted is reported below

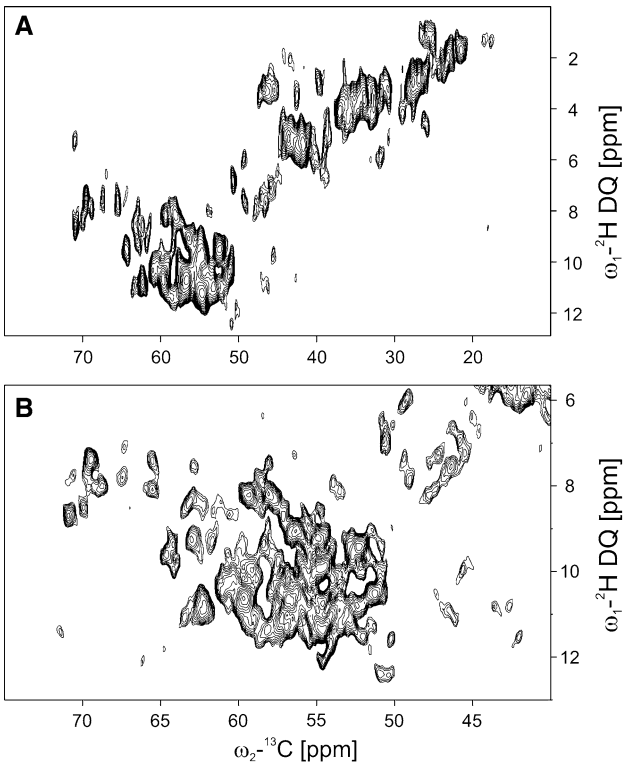

Fig. 5 $^{2}H_{DQ}$–^{13}C correlation spectrum of uniformly $^{2}H/^{13}C/^{15}N$ labeled OmpG, which was back-exchanged with 30/70% H_2O/D_2O. **a** The spectrum was processed with a squared sine function with a phase shift of $\pi/5$ in the indirect dimension while a Gauss-Lorentz function in the direct dimension was used with an exponential line broadening of −15 Hz and a Gaussian maximum of 0.03. **b** The 2D spectrum was processed in the same way as A, by utilizing forward linear-prediction with 32 additional output points in the deuterium indirect dimension

exploited to separate spin systems according to the chemical shifts of the $^{2}H_{DQ\alpha}$–$^{13}C_{\alpha}$ moieties. Several sets of threonine and serine cross peaks of the type $^{2}H_{DQ\alpha}$–$^{13}C_{\alpha}$–$^{13}C_{\beta}$ are present between 65 and 70 ppm and resolved along the $^{2}H_{DQ}$ frequency axis. However, in the 3D $^{2}H_{DQ}$–^{13}C–^{13}C– spectrum of OmpG, the $^{2}H_{DQ\alpha}$–$^{13}C_{\alpha}$–$^{13}C_{\beta,\gamma}$ and $^{2}H_{DQ\beta}$–$^{13}C_{\beta}$–$^{13}C_{\alpha/\gamma}$ transfers are strongly asymmetrical. Those amino acids whose $^{13}C_{\alpha}$ and $^{13}C_{\beta}$ chemical shifts are close to the rf carrier of the DREAM sweep show nearly symmetrical cross peaks, such as leucine, isoleucine, phenylalanine and tyrosine. The $^{2}H_{DQ\alpha}$–$^{13}C_{\alpha}$ and $^{2}H_{DQ\beta}$–$^{13}C_{\beta}$ strips of S134, L42 and L146 are shown in Fig. 7.

To provide a measure for the information content of the spectrum, we have counted the C_{α}–C_{β} and C_{β}–C_{α} correlations for Ala, Leu, Ser and Thr that show resolved signal sets in the 3D spectrum (Table SI2a-b) but in part strongly asymmetrical cross peak pattern. Out of ~90 resolved cross peaks, we have assigned 48 to the previously identified side chain carbon spin systems of the four residue types, Ala (*6*/15), Leu (*12*/19), Ser (*4*/12) and Thr (*12*/15) (*assigned*/number-of-residues, respectively). For residues with C_{β} chemical shifts in the range of 30–45 ppm, the cross-peak patterns are of substantial intensity and symmetrical. The $^{2}H_{DQ\alpha}$ and $^{2}H_{DQ\beta}$ chemical shifts of a number of residues (48 in total) which are sequentially assigned on the basis of our full OmpG data set are shown in the supplementary information, Table SI2b.

Discussion

Well-resolved ^{2}H–^{13}C 2D correlations and ^{2}H–^{13}C–^{13}C 3D spectra have been obtained from deuterated ubiquitin that was used as a test sample. Deuterium double-quantum line widths of 40–50 Hz (~0.4–0.5 ppm) were observed in the respective 2D $^{2}H_{DQ}$–^{13}C correlations from ubiquitine, enabling the separation of various overlapping carbon signal sets by making use of a third dimension. Even more surprisingly, well-resolved correlations with slightly broader linewidths (~0.8–1.1 ppm) were obtained of 2D-crystalline samples of the outer-membrane protein G from *E. coli*, demonstrating the applicability of the approach to large membrane proteins which are generally difficult to study. Moreover, higher sensitivity is achieved by the use

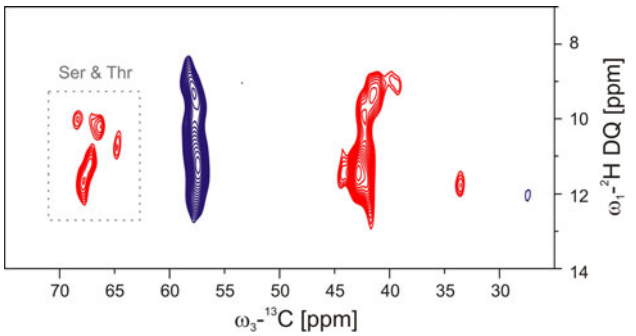

Fig. 6 A representative 2D plane extracted from the 3D $^2H_{DQ}$–^{13}C–^{13}C correlation spectrum of uniformly $^2H/^{13}C/^{15}N$ labeled OmpG. The plane was extracted at a ^{13}C chemical shift of 58.19 ppm. The diagonal peaks are represented in *blue*, the cross peaks in *red*

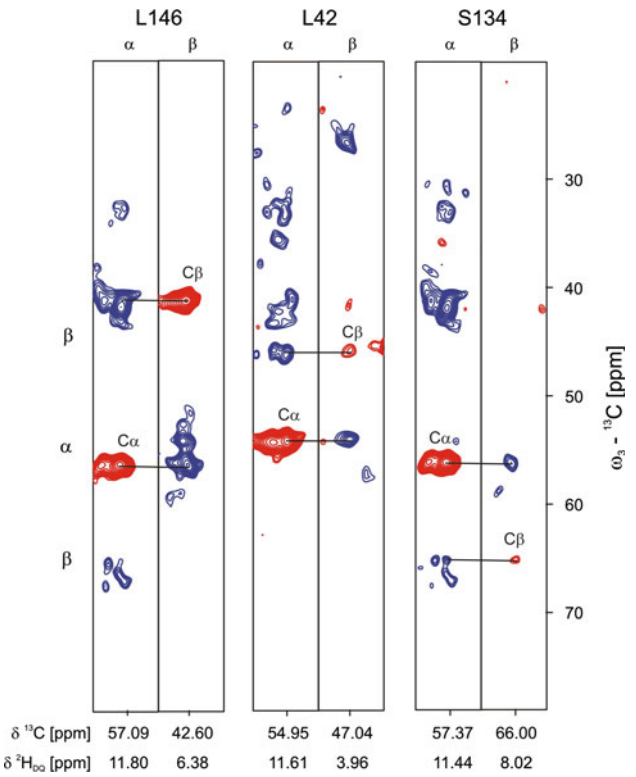

Fig. 7 Representative strip plots of the $^2H_{DQ}$–^{13}C–^{13}C spectrum of the uniformly $^2H/^{13}C/^{15}N$ labeled OmpG, showing intra-residue connectivities for residues L42, S134 and L146. *Blue* and *red* peaks are negative cross peaks and positive diagonal peaks, respectively. Each strip is extracted at the ^{13}C frequency reported at the *bottom*. The $^2H_{DQ}$ frequency of the plane from which strips are extracted is shown below

of initial ^2H–^{13}C CP in comparison to initial ^1H–^{13}C CP excitation in cases with less than 5% protons at side chain sites as observed for sparsely proton-containing perdeuterated SH3 (Akbey et al. 2011).

The $^2H_{DQ}$ linewidths observed for ubiquitine and OmpG proteins are promising, opening new perspectives when using the deuterium in a third spectral dimension. The values favorably compare to the proton linewidths observed for fully protonated proteins, which are in the order of ~1 ppm (Zhou et al. 2007). The use of homonuclear decoupling schemes can provide even better resolution, at the expense of lower sensitivity (Zhou et al. 2007). However, the proton linewidths observed for a fully deuterated protein with back-exchange ratios between 10 and 30% results in much narrower linewidths (~0.05 ppm at 400 MHz magnetic field) (Akbey et al. 2010b). Alternatively, proton content of the carbon sites can be tuned as shown recently (Asami et al. 2010), which increases the sensitivity at the initial polarization step. Nevertheless, at least similar sensitivity is obtained when applying the $^2H_{DQ}$ approach due to the use of all carbon sites, compared to the sparse labeling approaches.

This successful application has far-reaching consequences, since $^2H_{DQ}$ chemical shifts associated with side-chain moieties are thus accessible for use in assignment strategies using pulse sequences equivalent to those in solution NMR (HCCH–COSY and –TOCSY), enabling side-chain spin-system topologies using proton-like shifts to be resolved. This is important, since the tuning of the exchangeable proton content in the manner of Akbey et al. (2010b) may not always work, especially for membrane proteins, when back-exchange within the membrane-spanning portion is inefficient and refolding procedures cannot be applied. In this case, a structure determination concept relying solely on deuterons instead of protons is of highest importance. In fact, it can be envisaged that a fully deuterated protein in deuterated solvent will be most beneficially investigated for 3D-applications involving three different nuclei.

At first sight, excitation of deuterium, even in indirect dimensions, is disadvantageous in comparison to excitation of protons. First, the gyromagnetic ratio of deuterium is much lower than that of protons; second, the single-quantum lines of deuterium are generally broad. However, these disadvantages are compensated here by several factors: (1) the short deuterium T_1 allows high repetition rates and thus compensates for the lower Boltzmann polarization (40–100 ms), and (2) the favorable line width of deuterium double-quantum states leads to high resolution, with a surprisingly narrow effective line width in spectra of microcrystalline ubiquitin and OmpG. Accordingly, a 3D $^2H_{DQ}$–^{13}C–^{13}C correlation spectrum of a membrane protein (OmpG) is obtained in ~3.5 days. Side chain topologies of leucine, threonine, serine and other residues were analyzed by exploiting the proton-analogous $^2H_{DQ}$ chemical shifts to disperse the carbon–carbon correlation into a third dimension. The gain in resolution obtained in the $^2H_{DQ}$ dimension is striking. Three arguments can be invoked to explain the gain in resolution by utilizing $^2H_{DQ}$ instead of $^2H_{SQ}$: first, the resolution is increased due to evolution of double-quantum coherences (DQCs) while simultaneously

maintaining the absolute line width (Vega et al. 1976). Second, $^{2}H_{DQ}$ line widths are less sensitive to magic-angle offsets (Agarwal et al. 2009; Eckman et al. 1980; Hoffmann and Schnell 2004). Third, the $^{2}H_{DQ}$ line width is unaffected by dynamics which can exert a significant broadening on deuterium single-quantum coherences (SQCs) (Cavadini et al. 2008; Cutajar et al. 2006; Thrippleton et al. 2008).

Additional advantages can be ascribed to the use of highly deuterated samples. Coherence life times of carbons and, likewise, nitrogens become very long, up to over a hundred milliseconds (Akbey et al. 2010b; Linser et al. 2010; Schanda et al. 2009). Accordingly, transfer efficiencies in complex multidimensional experiments are higher and line widths are narrower. These long life times also open up possibilities for using scalar-coupling based transfer schemes, e.g. for transfer from C_{α} to CO. As another consequence, only modest decoupling is necessary, avoiding problems with sample heating and again allowing high repetition rates.

Conclusion

We have presented an approach that aims at the identification of amino acid side chain spin systems and demonstrated its use for large proteins. It may be envisaged that a combination of $^{2}H_{DQ}$–^{13}C spectroscopy with ^{1}H and ^{15}N may yield new opportunities for easing structure determination of biological macromolecules. The application of systematic proton dilution in an otherwise perdeuterated sample may offer a fourth nucleus for spectral editing purposes and detection with higher sensitivity. Such samples may be generated either by re-introducing only a fraction of protons at the exchangeable sites or by introducing individual protons at defined sites in the side chains of individual amino acids.

Our 3D $^{2}H_{DQ}$–^{13}C–^{13}C NMR spectroscopy approach also has another possible application in experiments which are performed at low temperatures, for example in the case of dynamic nuclear polarization (DNP) enhanced NMR experiments (Akbey et al. 2010a; Hall et al. 1997). We have recently shown that deuterated samples are very well suited for performing DNP-enhanced NMR experiments with better efficiency, resulting in higher enhancement factors than with purely protonated samples. In combination with the high-resolution deuterium frequency information that we utilize in the present work, such an approach holds promise to become a useful tool for obtaining atomic resolution information about challenging biological systems.

Acknowledgments Prof. Beat H. Meier is gratefully acknowledged for the measurement time provided at the 600 MHz magnet at ETH Zürich. AC and JR gratefully acknowledge Marie Cruie FP7-ITN (SBMP) funding (grant number 211800).

References

Agarwal V, Faelber K, Schmieder P, Reif B (2009) High-resolution double-quantum deuterium magic angle spinning solid-state NMR spectroscopy of perdeuterated proteins. J Am Chem Soc 131:2–3

Akbey U, Oschkinat H, van Rossum BJ (2009) Double-nucleus enhanced recoupling for efficient C-13 MAS NMR correlation spectroscopy of perdeuterated proteins. J Am Chem Soc 131:17054–17055

Akbey U, Franks WT, Linden A, Lange S, Griffin RG, van Rossum BJ, Oschkinat H (2010a) Dynamic nuclear polarization of deuterated proteins. Angew Chem Int Ed Engl 49:7803–7806

Akbey U, Lange S, Franks WT, Linser R, Rehbein K, Diehl A, van Rossum BJ, Reif B, Oschkinat H (2010b) Optimum levels of exchangeable protons in perdeuterated proteins for proton detection in MAS solid-state NMR spectroscopy. J Biomol NMR 46:67–73

Akbey U, Camponeschi F, van Rossum BJ, Oschkinat H (2011) Triple resonance cross-polarization for more sensitive 13C MAS NMR spectroscopy of deuterated proteins. Chemphysche 12: 2092–2096

Archer SJ, Bax A (1991) An alternative 3D-NMR technique for correlating backbone N-15 with side-chain H-beta-resonances in larger proteins. J Magn Reson 95:636–641

Asami S, Schmieder P, Reif B (2010) High resolution 1H-detected solid-state NMR spectroscopy of protein aliphatic resonances: access to tertiary structure information. J Am Chem Soc 132: 15133–15135

Bax A, Grzesiek S (1993) Methodological advances in protein NMR. Acc Chem Res 26:131–138

Bax A, Clore GM, Driscoll PC, Gronenborn AM, Ikura M, Kay LE (1990a) Practical aspects of proton-carbon-carbon-proton 3-dimensional correlation spectroscopy of C-13-labeled proteins. J Magn Reson 87:620–627

Bax A, Clore GM, Gronenborn AM (1990b) H-1-H-1 correlation via isotropic mixing of C-13 magnetization, a new 3-dimensional approach for assigning H-1 and C-13 spectra of C-13-enriched proteins. J Magn Reson 88:425–431

Bennett AE, Ok JH, Griffin RG, Vega S (1992) Chemical-shift correlation spectroscopy in rotating solids—radio frequency-driven dipolar recoupling and longitudinal exchange. J Chem Phys 96:8624–8627

Bockmann A, Gardiennet C, Verel R, Hunkeler A, Loquet A, Pintacuda G, Emsley L, Meier BH, Lesage A (2009) Characterization of different water pools in solid-state NMR protein samples. J Biomol NMR 45:319–327

Castellani F, van Rossum B, Diehl A, Schubert M, Rehbein K, Oschkinat H (2002) Structure of a protein determined by solid-state magic-angle-spinning NMR spectroscopy. Nature 420: 98–102

Cavadini S, Abraham A, Ulzega S, Bodenhausen G (2008) Evidence for dynamics on a 100 ns time scale from single- and double-quantum nitrogen-14 NMR in solid peptides. J Am Chem Soc 130:10850–10851

Chandrakumar N, von Fricks G, Gunther H (1994) The 2D quadshift experiment—seperation of deuterium chemical-shifts and quadrupolar couplings by 2-dimensional solid-state MAS NMR-spectroscopy. Magn Reson Chem 32:433–435

Chevelkov V, Rehbein K, Diehl A, Reif B (2006) Ultrahigh resolution in proton solid-state NMR spectroscopy at high levels of deuteration. Angew Chem Int Ed Engl 45:3878–3881

Cutajar M, Ashbrook SE, Wimperis S (2006) H-2 double-quantum MAS NMR spectroscopy as a probe of dynamics on the microsecond timescale in solids. Chem Phys Lett 423:276–281

De PG, Lewandowski JR, Loquet A, Bockmann A, Griffin RG (2008) Proton assisted recoupling and protein structure determination. J Chem Phys 129:245101

Eckman R, Muller L, Pines A (1980) Deuterium double-quantum NMR with magic angle spinning. Chem Phys Lett 74:376–378

Ernst M, Detken A, Bockmann A, Meier BH (2003) NMR spectra of a microcrystalline protein at 30 kHz MAS. J Am Chem Soc 125:15807–15810

Fesik SW, Eaton HL, Olejniczak ET, Zuiderweg ER, McIntosh LP, Dahlquist FW (1990) 2D and 3D NMR-spectroscopy employing C-13–C-13 magnetization transfer by isotropic mixing—spin systems-identification in large proteins. J Am Chem Soc 112: 886–888

Grzesiek S, Bax A (1992) Correlating backbone amine and side-chain resonances in larger proteins by multiple relayed triple resonance NMR. J Am Chem Soc 114:6291–6293

Hall DA, Maus DC, Gerfen GJ, Inati SJ, Becerra LR, Dahlquist FW, Griffin RG (1997) Polarization-enhanced NMR spectroscopy of biomolecules in frozen solution. Science 276:930–932

Hiller M, Krabben L, Vinothkumar KR, Castellani F, van Rossum BJ, Kuhlbrandt W, Oschkinat H (2005) Solid-state magic-angle spinning NMR of outer-membrane protein G from *Escherichia coli*. Chembiochem 6:1679–1684

Hoffmann A, Schnell I (2004) Two-dimensional double-quantum 2H NMR spectroscopy in the solid state under OMAS conditions: correlating 2H chemical shifts with quasistatic line shapes. Chemphyschem 5:966–974

Huang KY, Siemer AB, McDermott AE (2011) Homonuclear mixing sequences for perdeuterated proteins. J Magn Reson 208: 122–127

Igumenova TI, Wand AJ, McDermott AE (2004) Assignment of the backbone resonances for microcrystalline ubiquitin. J Am Chem Soc 126:5323–5331

Ikura M, Kay LE, Bax A (1991) Improved three-dimensional 1H–13C–1H correlation spectroscopy of a 13C-labeled protein using constant-time evolution. J Biomol NMR 1:299–304

Jehle S, Rajagopal P, Bardiaux B, Markovic S, Kuhne R, Stout JR, Higman VA, Klevit RE, van Rossum BJ, Oschkinat H (2010) Solid-state NMR and SAXS studies provide a structural basis for the activation of alphaB-crystallin oligomers. Nat Struct Mol Biol 17:1037–1042

Kay LE, Ikura M, Tschudin R, Bax A (1990) 3-dimensional triple-resonance nmr-spectroscopy of isotopically enriched proteins. J Magn Reson 89:496–514

Keller R, Wuthrich K (2002) A new software for the analysis of protein NMR spectra

Kristensen JH, Bildsoe H, Jakobsen HJ, Nielsen NC (1999) Separation of (2)H MAS NMR spectra by two-dimensional spectroscopy. J Magn Reson 139:314–333

Lange A, Giller K, Hornig S, Martin-Eauclaire MF, Pongs O, Becker S, Baldus M (2006) Toxin-induced conformational changes in a potassium channel revealed by solid-state NMR. Nature 440: 959–962

Lee YK, Kurur ND, Helmle M, Johannessen OG, Nielsen NC, Levitt MH (1995) Efficient dipolar recoupling in the NMR of rotating solids. A sevenfold symmetric radiofrequency pulse sequence. Chem Phys Lett 242:304–309

Leskes M, Akbey U, Oschkinat H, van Rossum BJ, Vega S (2011) Radio frequency assisted homonuclear recoupling—a Floquet description of homonuclear recoupling via surrounding heteronuclei in fully protonated to fully deuterated systems. J Magn Reson 209:207–219

Linser R, Fink U, Reif B (2008) Proton-detected scalar coupling based assignment strategies in MAS solid-state NMR spectroscopy applied to perdeuterated proteins. J Magn Reson 193:89–93

Linser R, Fink U, Reif B (2010) Narrow carbonyl resonances in proton-diluted proteins facilitate NMR assignments in the solid-state. J Biomol NMR 47:1–6

Rienstra CM, Tucker-Kellogg L, Jaroniec CP, Hohwy M, Reif B, McMahon MT, Tidor B, Lozano-Perez T, Griffin RG (2002) De novo determination of peptide structure with solid-state magic-angle spinning NMR spectroscopy. Proc Natl Acad Sci USA 99:10260–10265

Sattler M, Schleucher J, Griesinger C (1999) Heteronuclear multidimensional NMR experiments for the structure determination of proteins in solution employing pulsed field gradients. Prog Nucl Magn Reson Spectrosc 34:93–158

Schanda P, Huber M, Verel R, Ernst M, Meier BH (2009) Direct detection of (3 h)J(NC') hydrogen-bond scalar couplings in proteins by solid-state NMR spectroscopy. Angew Chem Int Ed Engl 48:9322–9325

Schnell I, Spiess HW (2001) High-resolution 1H NMR spectroscopy in the solid state: very fast sample rotation and multiple-quantum coherences. J Magn Reson 151:153–227

Scholz I, Huber M, Manolikas T, Meier BH, Ernst M (2008) MIRROR recoupling and its application to spin diffusion under fast magic-angle spinning. Chem Phys Lett 460:278–283

Schubert M, Manolikas T, Rogowski M, Meier BH (2006) Solid-state NMR spectroscopy of 10% 13C labeled ubiquitin: spectral simplification and stereospecific assignment of isopropyl groups. J Biomol NMR 35:167–173

Shaka AJ, Keeler J, Frenkiel T, Freeman R (1983) An improved sequence for broad-band decoupling—WALTZ-16. J Magn Reson 52:335–338

Takegoshi K, Nakamura S, Terao T (2003) C-13-H-1 dipolar-driven C-13-C-13 recoupling without C-13 rf irradiation in nuclear magnetic resonance of rotating solids. J Chem Phys 118: 2325–2341

Thrippleton MJ, Cutajar M, Wimperis S (2008) Magic angle spinning (MAS) NMR linewidths in the presence of solid-state dynamics. Chem Phys Lett 452:233–238

Vega S, Shattuck TW, Pines A (1976) Fourier-transform double-quantum NMR in solids. Phys Rev Lett 37:43–46

Verel R, Ernst M, Meier BH (2001) Adiabatic dipolar recoupling in solid-state NMR: the DREAM scheme. J Magn Reson 150: 81–99

Wasmer C, Lange A, Van MH, Siemer AB, Riek R, Meier BH (2008) Amyloid fibrils of the HET-s(218–289) prion form a beta solenoid with a triangular hydrophobic core. Science 319: 1523–1526

Zhou DH, Shah G, Cormos M, Mullen C, Sandoz D, Rienstra CM (2007) Proton-detected solid-state NMR spectroscopy of fully protonated proteins at 40 kHz magic-angle spinning. J Am Chem Soc 129:11791–11801